

Article

# Early Jurassic Gypsum within Eastern African Continental Marginal Basins and Its Significance for Gas Play

Jun Cai <sup>1,2,3,\*</sup> and Rong Guo <sup>1,2</sup>

<sup>1</sup> Cooperative Innovation Center of Unconventional Oil and Gas, Yangtze University (Ministry of Education & Hubei Province), Wuhan 430100, China; grcjd@163.com

<sup>2</sup> Key Laboratory of Exploration Technologies for Oil and Gas Resources, Ministry of Education, Yangtze University, Wuhan 430100, China

<sup>3</sup> Key Laboratory of Polar Geology and Marine Mineral Resources (China University of Geosciences, Beijing), Ministry of Education, Beijing 100083, China

\* Correspondence: caijun.jz@163.com

**Abstract:** Although the eastern African continental marginal basins have discovered giant gas fields, it is not clear whether the Early Jurassic gypsum associated with the main source rocks controls the gas play. In this paper, we use well logging, seismic reflection, and organic geochemistry data to synthesize the distribution and origin of the gypsum deposits and their control over the gas play. The results show that from 201 Ma to 183 Ma, a thick suite of mudstone with thin-layered gypsum began to form in the southern gulf-like sea due to water stratification. With the sea level falling since 183 Ma, a thick suite of gypsum was deposited in some grabens, where the sedimentary environment changed to lagoons. The gypsum increases the maturity threshold depth of Lower Jurassic source rocks and delays the peak time of gas generation, resulting in the ongoing filling of East African natural gas reservoirs and the formation of giant reserves. In addition, the gypsum not only controls the distribution of conventional gas but also makes the Lower Jurassic shale, where the faults are not developed, an important place for shale gas exploration in the future due to the good sealing properties of the gypsum.

**Keywords:** gypsum; depositional model; shale gas; conventional gas; eastern African continental margin



**Citation:** Cai, J.; Guo, R. Early Jurassic Gypsum within Eastern African Continental Marginal Basins and Its Significance for Gas Play. *J. Mar. Sci. Eng.* **2024**, *12*, 93. <https://doi.org/10.3390/jmse12010093>

Academic Editor: George Kontakiotis

Received: 10 November 2023

Revised: 22 December 2023

Accepted: 22 December 2023

Published: 2 January 2024



**Copyright:** © 2024 by the authors. Licensee MDPI, Basel, Switzerland. This article is an open access article distributed under the terms and conditions of the Creative Commons Attribution (CC BY) license (<https://creativecommons.org/licenses/by/4.0/>).

## 1. Introduction

Gypsum deposits have always been one of the hot research topics due to their usage in many industries (e.g., chloralkali industry, fertilizer industry) [1]. For a few decades, gypsum has gained much attention in the petroleum industry because of its controls on oil and gas generation and accumulations worldwide [2]. The Bohai Bay Basin [3,4], the Ordos Basin [5,6], the Jiangnan Basin [7], the Songliao Basin [8,9], the Lower Congo Basin [10], the Persian Gulf [11,12], the Pricaspian [13], the African passive continental margin [14,15], the Brazilian deep-water basins [16,17], and the Tarim Basin [18], all have significant petroleum plays.

Despite the multiple achievements mentioned above, there have been relatively few publications on the gypsum deposited in the eastern African continental marginal basins, which has been considered to be the world's largest increase in natural gas reserves in the last decade. It is currently known that the gypsum is associated with the main source rocks of the eastern African continental marginal basins, which are considered to be the Early Jurassic mudstone [19]. Unfortunately, the distribution range of the gypsum still needs to be solved, which further limits the understanding of controlling its effects on gas play. In this paper, we attempt to clarify the distribution range, establish an appropriate sedimentary model for the Early Jurassic gypsum deposits, and finally discuss its controlling effects on gas play.

## 2. Geological Background

The eastern African continental margin is composed of several basins stretching from north to south, including the Somalia Basin, Lamu Basin, Tanzania Basin, Ruvuma Basin, Mozambique Basin, Mulongdawa Basin, and Mazenga Basin, with a total sedimentary area of about  $3.7 \times 10^6 \text{ km}^2$  (Figure 1). Our research area focuses on the Rovuma, Tanzania, and Lamu Basins due to abundant seismic data availability.

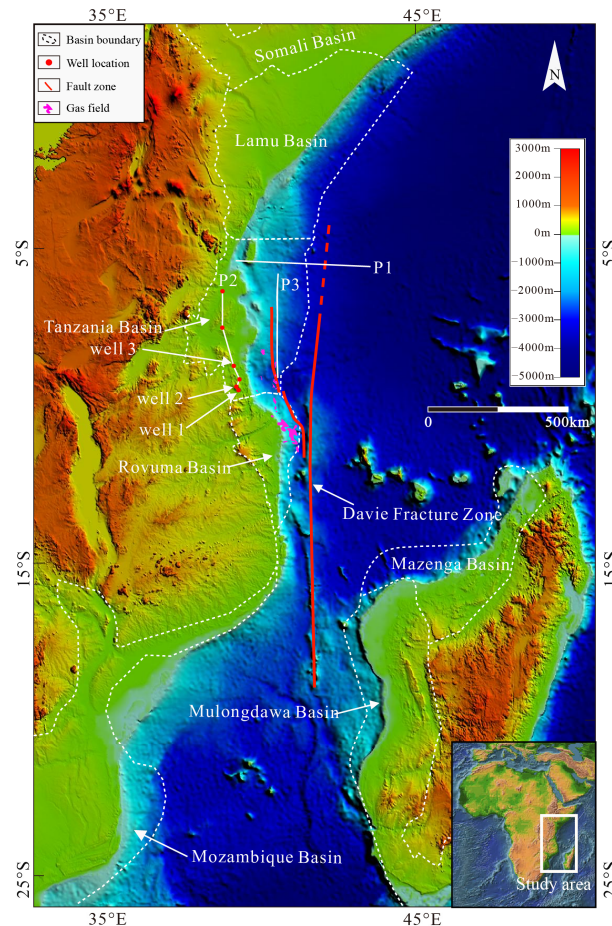


**Figure 1.** The map shows the locations of the Somalia Basin, Lamu Basin, Tanzania Basin, Ruvuma Basin, Mozambique Basin, Mulongdawa Basin, and Mazenga Basin. The basin locations were referred to by [20].

The eastern African continental marginal basins are developed in the basement of the Carboniferous crystalline rock, with a basinal depositional thickness of more than 10 km. Its tectonic evolution can be divided into three stages: the intracontinental rift stage, the intercontinental rift stage, and the passive continental margin stage. The first stage initiates from the late Carboniferous to the Triassic. Along with the gradual formation of the Gondwana continent, a strong “mantle plume” rose beneath the southeast of the continent, causing regional crustal uplifting, faulting, and volcanic activity, forming a widely distributed intracontinental basin where a set of fluvial, lacustrine, and marshy facies were formed [21]. Since the strata deposited during the intercontinental rifting are best preserved in the Kaloo basin within South Africa, this period is also known as the Kaloo Rift Valley and is represented by the Kaloo Group deposits as a tectonic event affecting the entire Gondwana continent [22]. The profile reveals that the structural style of this period is dominated by a wide range of horsts, grabens, and half-grabens (Figure 2a).

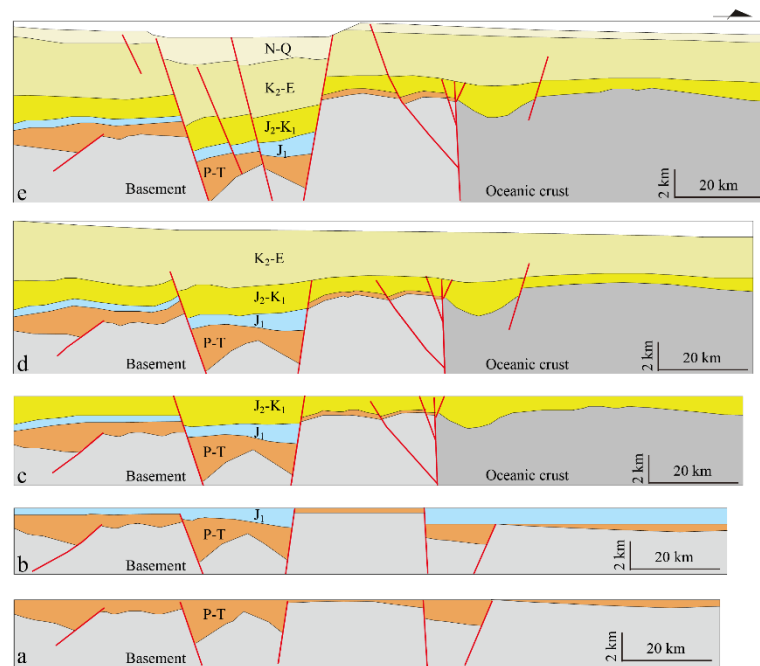


**Figure 2.** (a) The diagram presents the tectonic structure and sedimentary fill of the eastern African continental margin at the intracontinental rift stage; (b) The diagram presents the tectonic structure and sedimentary fill at the intercontinental rift stage; (c) The diagram presents the tectonic structure and sedimentary fill from the Middle Jurassic to the Early Jurassic; (d) The diagram presents the tectonic structure and sedimentary fill from the Upper Jurassic to the Paleogene; (e) The diagram presents the tectonic structure and sedimentary fill from the Neogene to the present. Abbreviations: P-T, Permian to Triassic; J<sub>1</sub>: Lower Jurassic; J<sub>2</sub>-K<sub>1</sub>: Middle Jurassic to Lower Cretaceous; K<sub>2</sub>-E: Upper Cretaceous to Paleogene; N-Q: Neogene to Quaternary.

The second stage begins with the Early Jurassic. The Gondwana continent began to break up into several different blocks from northwest to southeast, where seafloor spreading and drifting are limited to the northeast, resulting in large-scale rifting and subsidence occurring in present-day coastal areas of Somalia, Kenya, Tanzania, and Madagascar, causing seawater flooding from the northeast and the formation of narrow bays similar to the Red Sea [23]. The seismic profiles reveal that the structural style is dominated by strata filling, but a small number of preexisting faults have been reactivated under the regional extensional stress field, resulting in graben formation (Figure 2a,b), showing that this period is dominated by thermal subsidence with limited normal faulting over most of the basins.

In the middle Jurassic, the Gondwana continent was split into two continents, the East and the West. The entire East African Sea began to prograde into the passive continental margin stage [24], which could be further divided into three secondary stages according to the sub-tectonic events. From the middle Jurassic to the early Cretaceous, the continents of Madagascar and East Gondwana broke away from the African continent and drifted southward along the Davie fracture zone characterized by dextral strike-slipping, resulting in a dextral shear continental margin on the southern margin of East Africa [25]. From the late Cretaceous to the Eocene, the tectonic activity of the East African continental margin was weak (Figure 2d), with a set of shallow sea and delta deposits [26]. From the Oligocene, due to the activity of the Afar mantle plume in northern East Africa, with accelerated subsidence in the central part of the eastern African continental margin and relative uplift of the eastern Davie fracture zone (Figures 2e and 3), the East African Rift began to form [27].

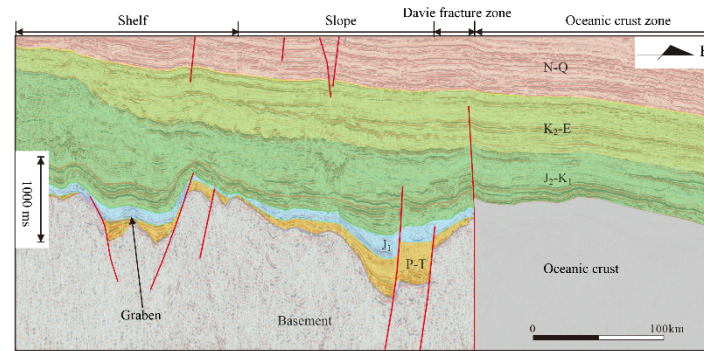


**Figure 3.** The interpreted seismic profile reveals the tectonic framework of the Lower Jurassic within the eastern African continental margin. The red line presents the fault. See P1 for the location.

### 3. Materials and Methods

The analysis of the vertical distribution of the Early Jurassic gypsum deposits were primarily based on the data from the drilling and logging of six wells. Considering the heterogeneous distribution of the rock and the few drillings in the deep-water encounter of the Lower Jurassic, a large amount of seismic data were used to classify seismic sequences and seismic facies. The main method is to obtain the petrophysical parameters of the Lower Jurassic, including the densities, interval velocities, and wave impedance characteristics of mudstone, sandstone, and gypsum deposits, based on logging data, which could better utilize seismic reflections in seismic profiles across key wells to establish connections with lithology. Then, in areas without wells, the planar distribution of the gypsum can be inferred based on similar seismic facies. Notably, during our interpretation of the seismic data, we reviewed strata and structural models from unpublished research reports and published literature to obtain biostratigraphic and chemostratigraphic constraints on the age of seismic stratigraphy from key selected wells. In addition, in discussing the sedimentary environment, more than 100 mudstone samples were collected to measure the values of the total organic carbon (TOC) and hydrogen index (HI), and the detailed analytical procedure and accuracy follow [28].

### 4. Results

#### 4.1. Vertical Distribution of the Gypsum Deposits

Drilling records show that the Lower Jurassic succession could be divided into the lower and upper parts based on the difference in lithology. The lower part is dominated by a thick suite of mudstone with thin-layered gypsum. The upper part is dominated by a thick suite of gypsum deposits with thin layers of mudstone. For example, the lower part of the Lower Jurassic succession of well 1, located within the southern Tanzanian Basin toward land, are mainly mudstone with scarce gypsum layers based on the data from drilling and logging (Figure 4). The gamma-ray curve is finger-shaped, while the acoustic curve is at middle amplitude, which could be considered to be the shallow marine deposits. The gamma-ray curve of the upper part of the Lower Jurassic succession is in the shape of a gearbox and low-amplitude funnel, which is significantly different from the lower part of the Jurassic succession. Combined with data from drilling and logging, the lithology within this part are dominated by a thick suite of gypsum with thin layers of mudstone. The gypsum percentage increases, while the mudstone component decreases. Well 2 has similar characteristics to well 1 (Figure 4), the Lower Jurassic of which can also be divided in two parts vertically, the lower and the upper part of the Lower Jurassic sequence. The lower part of the Lower Jurassic succession is shallow marine-thick siliciclastic mudstone with thin layers of gypsum, while the upper part of the Lower Jurassic succession is presented by thick gypsum deposits. It should be noted that red gypsum deposits appear in the upper part of the Lower Jurassic succession.

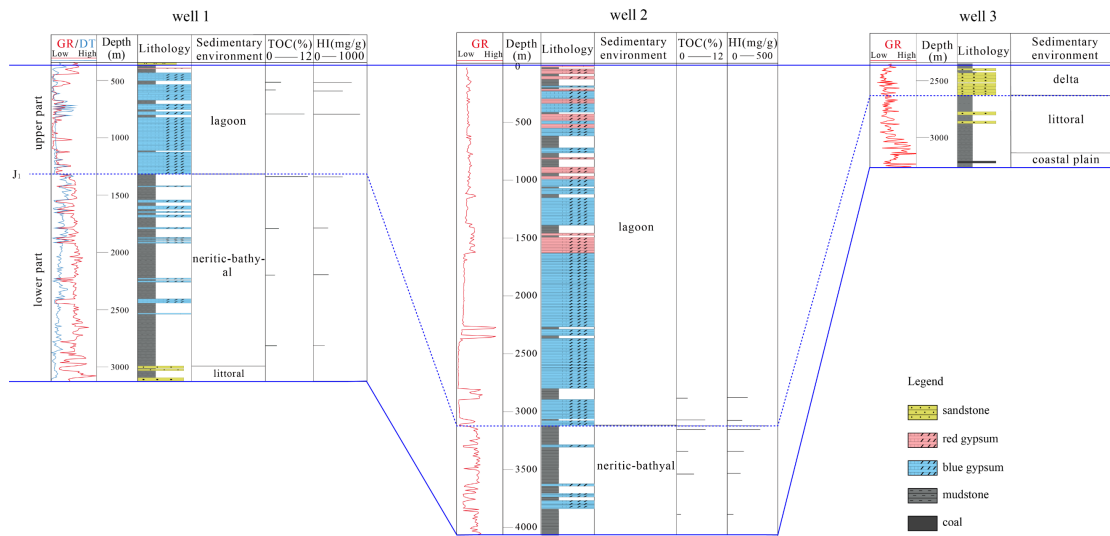


**Figure 4.** Regional Lower Jurassic stratigraphy across well 1, well 2, and well 3 within the eastern African continental margin. GR: gamma curve; DT: acoustic curve; TOC: total organic carbon; HI: hydrogen index. See P2 for the locations of well 1, well 2, and well 3.

**4.2. Planar Distribution of the Gypsum Deposits**

More drilling records reveal the heterogeneity of gypsum distribution. For example, according to well 3 (Figure 4), in the Lower Jurassic, with a 19 m-thick black coal seam at the bottom, a thick suite of mudstone upward, and sandstone at the top, gypsum was not observed within well 3 (Figure 4). The results show that the values of acoustic logging of the Lower Jurassic sandstone are mainly concentrated around 225  $\mu\text{s/m}$ , with mudstone around 315  $\mu\text{s/m}$  and gypsum around 200  $\mu\text{s/m}$  (Figure 5), indicating that mudstone exhibits low-speed characteristics, while sandstone and gypsum exhibit high-speed characteristics. The results from logging data show that the average velocity in sandstone are 2620  $\text{kg/m}^3$ , with gypsum being 2070  $\text{kg/m}^3$ , and mudstone being 2420  $\text{kg/m}^3$  (Table 1). The wave impedance of rock is equal to the product of longitudinal wave velocity and density. The calculation results show that the wave impedance of gypsum is about  $900 \times 10^4 \text{ kg/(s}\cdot\text{m)}$ , with sandstone about  $1164 \times 10^4 \text{ kg/(s}\cdot\text{m)}$ , and mudstone about  $768.35 \times 10^4 \text{ kg/(s}\cdot\text{m)}$  (Table 1), indicating that the wave impedance of mudstone is low, the wave impedance of sandstone is high, and the wave impedance of gypsum is between mudstone and sandstone. If it is a thick suite of layered gypsum with thin-layered mudstone, the seismic facies would be characterized by high amplitude and continuous reflectance. If it is a thick suite of mudstone with thin-layered gypsum, it would be characterized by continuous parallel weak reflection or bland reflection. Due to the significant wave impedance difference between mudstone and sandstone, interbedded sandstone-mudstone would be characterized by strong reflection.

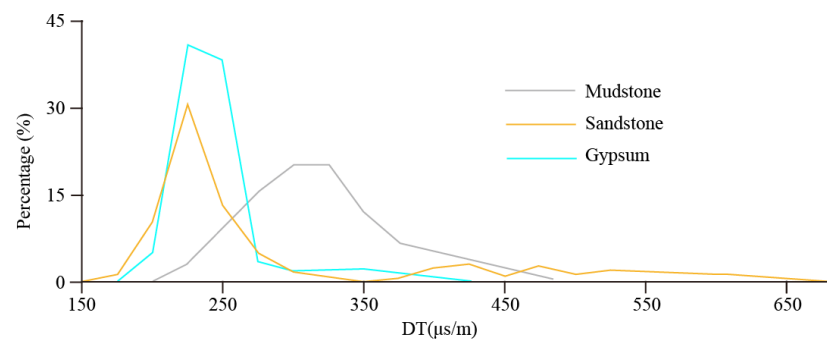


**Figure 5.** The diagram shows the distribution frequency of interval transit time in different Lower Jurassic lithologies.

**Table 1.** The average rock mechanics parameters of the Lower Jurassic.

Lithology	DT ( $\mu\text{s/m}$ )	Velocity (m/s)	Density ( $\text{kg/m}^3$ )	Wave Impedance ( $\text{kg/(s}\cdot\text{m)}$ )
sandstone	225	4444	2620	$1164.33 \times 10^4$
gypsum	230	4348	2070	$900 \times 10^4$
mudstone	315	3175	2420	$768.35 \times 10^4$

The seismic profiles through the key wells confirm the above speculation. For example, the seismic profile across well 1 indicates that the whole Lower Jurassic seismic facies could be divided into three parts: the lowest part is characterized by weakly continuous strong reflection corresponding to the sandstone-mudstone intercalation at the bottom of the Lower Jurassic, the middle part is characterized by weak reflection corresponding to the thick suite of mudstone with thin layers of gypsum, and the upper part is characterized by continuous strong reflection corresponding to the thick suite of gypsum deposits with thin layers of mudstone (Figure 6). The more seismic data show that most Lower Jurassic succession are characterized by weak reflection (Figure 7), while the Lower Jurassic in the nearshore and the northern edge of the Tanzania Basin, as well as the Lamu Basin, is characterized by weakly continuous strong reflections. It is notable that in some nearshore grabens, the Lower Jurassic succession is characterized by weak reflections in the lower part and continuous, strong reflections in the upper part.

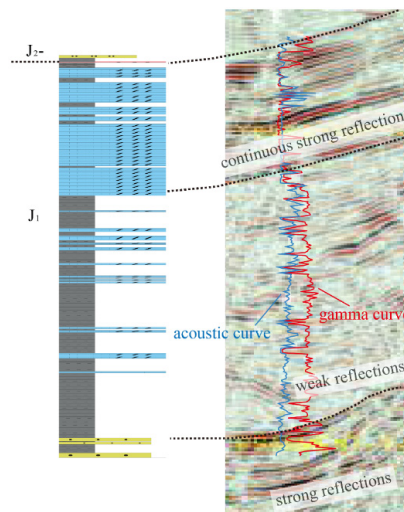


**Figure 6.** The through-well 1 seismic profile indicates that the whole Lower Jurassic seismic facies could be divided into three parts.

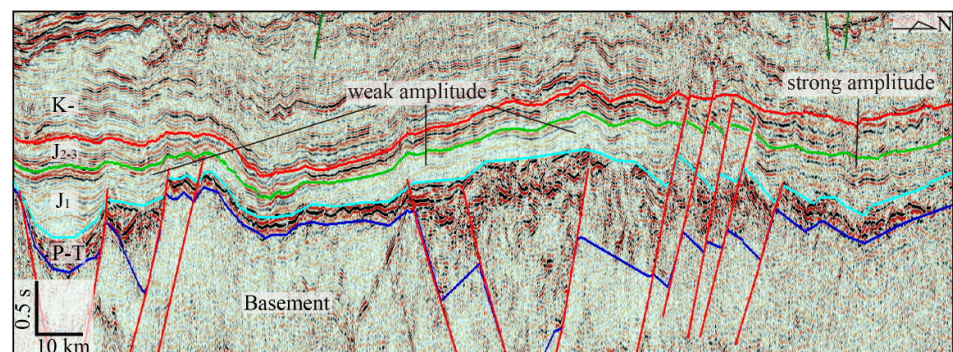


**Figure 7.** The seismic profile shows that the Lower Jurassic is characterized by weak reflections, while the northern part is characterized by weakly continuous, strong reflections. Different color lines present stratigraphic boundaries and faults. See P3 for the location.

#### 4.3. Variations of the TOC and HI

Although the TOC values change greatly, as could be seen from Figure 8, the major TOC values within the northern wells range from 1.3% to 2.2%, while the TOC values within the southern wells range from 5.1% to 6.1%, which shows that the TOC values within the southern wells are much higher than those within the northern wells. The HI values have a phenomenon similar to the TOC values. The average HI values within the northern wells range from 96 mg/g to 133 mg/g, while the average HI values within the southern part range from 276 mg/g to 836 mg/g (Figure 8).

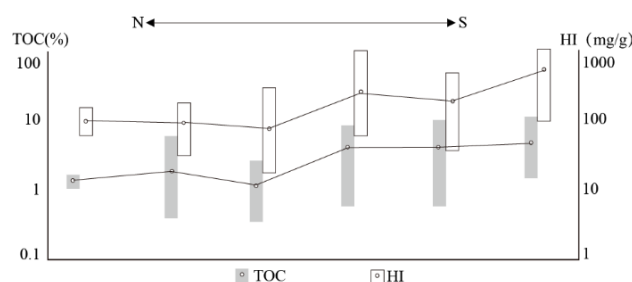


**Figure 8.** Box- and whisker plots show the range and average values of the TOC values and the HI values. See Figure 1 for the location of the wells.

## 5. Discussion

### 5.1. Sea Level Changes

Two main reasons could account for the differential distribution of gypsum deposits: the plastic rheology of gypsum and the differential sedimentary environment, respectively. Considering that there is no evidence of large-scale plastic rheology of gypsum on the seismic profiles within the eastern African continental marginal basins, the difference in sedimentary environment is the main controlling factor of the differential gypsum distribution. Because sea level change plays an important role in controlling the sedimentary environment, it is necessary to discuss sea level change within the eastern African continental marginal basins to clarify the sedimentary environment. The gamma-ray curve of the Lower Jurassic within well 3 is mainly bell-shaped and funnel-shaped, and a 19 m-thick black coal seam at the bottom of the Lower Jurassic reflects that the initial environment may be a coastal plain, followed by the littoral sea and delta inferred by the upward-changing lithology. Environmental changes show a sea level rise during the early stage of the Early Jurassic, followed by a sea level fall during the late stage of the Early Jurassic. The presumption could also be evidenced by seismic stratigraphy. The stacking geometry of the Lower Jurassic in seismic profiles also enables a two-fold division. The lower is composed of a wedge-shaped body onlapping and converging to the east in a direction to the Davie fracture ridge (Figures 1 and 3). This retrogradational stacking pattern and reversal of the convergence direction are attributed to transgressive deposits that accumulate mainly in areas adjacent to the shoreline, resulting in a cut-off of sediment supply to the marine environment. Therefore, it indicates a rapid sea level rise that creates coastal accommodation faster than sediment can fill it [29,30]. The overlying section is defined by a series of offlapping clinoforms that step down into the basin (Figure 9). Such a basinward shift and the lack of topset aggradation may be caused by progradation during a relative sea-level fall.

The above analysis suggests that the eastern African continental margin experienced a rapid sea level rise during the early stage of the Early Jurassic, followed by a sea level fall during the late stage of the Early Jurassic. Both changes coincide with those of the global sea level change [31], which can be seen as the global sea level rise from 201 Ma to 183 Ma, followed by the sea level fall. Thus, we interpret that the Early Jurassic strata within this continental margin experienced a sea level rise of about 18 Ma and a sea level fall of about 12 Ma.

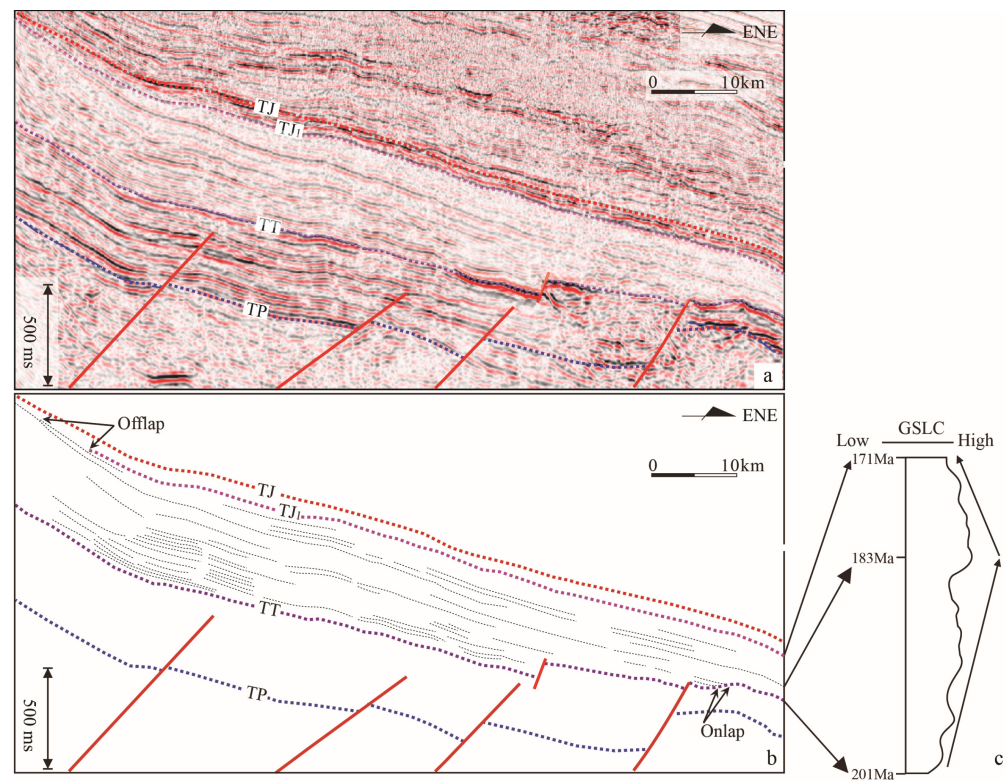


**Figure 9.** (a) Seismic profile and (b) geological profile showing the retrogradation and marine onlap at the early stage of the Early Jurassic and the offlap pattern at the late stage. TP: top of Permian; TT: top of Triassic; TJ<sub>1</sub>: top of Lower Jurassic; TJ: top of Jurassic. (c) Shows the global sea level change curve during the Early Jurassic [31].

### 5.2. Changes in the Sedimentary Environment through the Early Jurassic

During the Early Jurassic, with the break-up of the eastern Gondwana continent and the western Gondwana continent in a “V” shape from the northeast (Figure 10a), the Paleo-Tethys Ocean began to form from northeast to southwest, forming a gulf-like sea [22,23,32,33]. Northern Tanzania and Lamu Basins were close to the open sea, where they had a strong capacity for water exchange, while southern Tanzania and Rovuma Basins were relatively far away from the open sea environment with weak water circulation, resulting in an increase in reducibility from northeast to southwest.

The organic geochemical data related to source rocks supports the above opinion. The TOC could reflect the degree of the organic matter enrichment. Statistics indicate that the overwhelming majority of global organic matter is degraded during sedimentation, and the proportion preserved is less than 0.5% [34]. Thus, the preservation condition of organic matter is an important main controlling factor of organic matter enrichment [24,35,36]. Demaison & Moore [36] calculated the primary productivities of the global ocean and the TOC distributions in seabed sediments and found that the source rock distribution was critically affected by the redox degree of the water. Additionally, the organic-rich source rocks developed in the deep sea. Such environments existed in the lower Cretaceous of the Atlantic Ocean and the Pacific Ocean. In such environments, there is evidence of reductive conditions and the preservation of organic matter [37]. The Kivu Lake in eastern Africa [38], the Black Sea [39], the Bohai Bay Basin in eastern China [40], and the Bayingebi Basin in eastern China [41]. Wei & Jiang [41] also suggest that the preservation condition is the main controlling factor of organic matter enrichment. Moreover, the preservation condition of modern sedimentary settings is also a major factor controlling organic matter enrichment [37,42]. The content of organic carbon in a reducing environment is generally 1.0% to 20.0%, while the TOC values in an oxic environment are lower, ranging from 0.2% to 4.0% [37]. For example, although Albert Lake exhibits the highest productivity among

the four lakes within the western part of the Eastern African Rift Valley, the TOC value in the surface sediments is the lowest [42]. The reason is that Albert Lake is in an oxic environment with frequent water turbulence, where it is difficult for organic matter to be buried [42]. If the reducibility increases from the northeast of the gulf-like sea to the southwest, the preservation of organic matter within the southwestern part of the gulf-like sea is much better than that within the northeastern part. Thus, it can be speculated that the average TOC values within the southwestern part are higher than those within the northeastern part, which is in line with the variations of the measured TOC values (Figure 8). In addition, the HI is the ratio of the amount of pyrolytic hydrocarbon to the total organic carbon, which is generally used to reflect the organic matter type and can also indicate the capacity of preservation of organic matter after deposition [43]. The high value of HI represents that the bottom of the water with a strong capacity for organic matter preservation is in a reducing environment, while the low value of HI represents a relative oxic environment [43]. Considering the consistent organic matter type of the Early Jurassic source rock within the Tanzania Basin [19], the variations in the HI values are likely controlled by differences in preservation conditions. The measured results of the HI values also suggest that the reducibility within the southern part is better than that within the northern part (Figure 8).

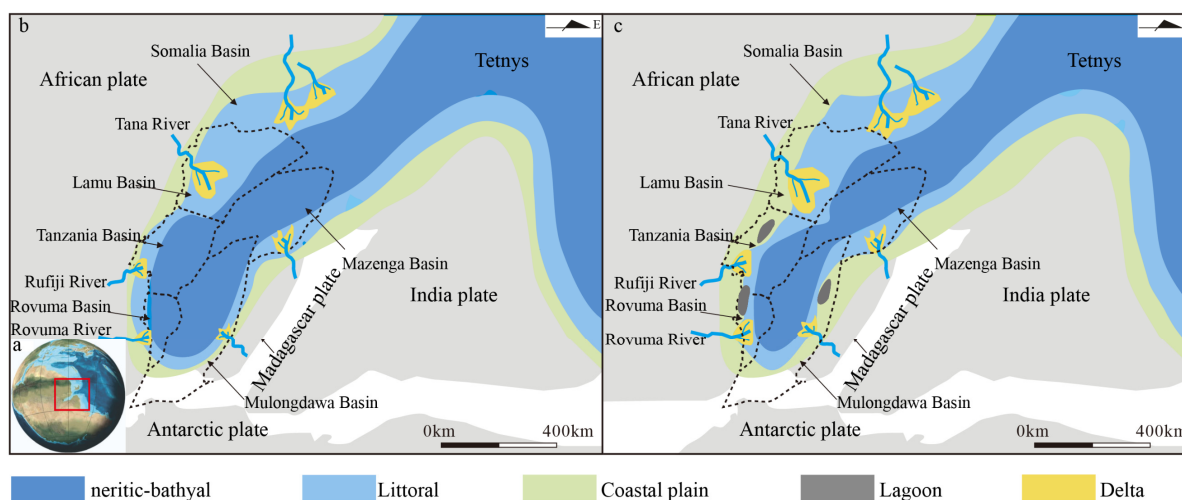


**Figure 10.** (a) A global paleogeographical map showing the paleogeographic reconstruction during the Early Jurassic. (b) The map shows the sedimentary environment at the early stage of the Early Jurassic; (c) The map shows the sedimentary environment at the late stage of the Early Jurassic. The reconstructed paleo-plate pattern and paleo-sedimentary environment refer to [22,23,32,33].

The Early Jurassic of the eastern African continental marginal basins consists of several lithological changes. The succession begins with a thick suite of mudstone with thin-layered gypsum, followed by a thick suite of gypsum deposits with thin layers of mudstone. TOC values increase gradually from bottom to top, and the HI values have similar characteristics (Figure 4), reflecting the possibility of gradually increasing reducibility. For the thick suite of gypsum deposits with thin layers of mudstone, the values of both TOC and HI remain at a relatively high level initially, with a decrease at the top, probably indicating strong reducibility in the early stage and later oxidation enhancement, which corresponds to the increase of red gypsum deposits within the upper part of the Lower Jurassic succession (e.g., well 1 and well 2).

Based on the analysis above, combined with data from drillings and seismic, unpublished research reports, and published literature [20,23], four types of sedimentary environments from 201 Ma to 183 Ma are identified, including delta, coastal plain, littoral, and neritic-bathyal environments (Figure 10b). During the period of sea level rise, the lagoon appears (Figure 10c).

### 5.3. Depositional Model

There are presently two main genetic models accounting for the formation of gypsum deposits. The first is the shallow water genetic model, which suggests that in a relatively closed sedimentary environment under arid climate conditions, the water is concentrated and gypsum is precipitated due to prevailing water evaporation over water influx [1,44,45]. The other is the deep water model [46–50], which considers water stratification resulting in the formation of gypsum deposits [51]. A dominant control on whether water bodies are well stratified or mixed is depth. Brainerd and Gregg [51] propose that waves generated by winds at the air-water surface will mix downward to the bottom of the waves, forming a mixed layer. The maximum depth of a mixed layer was marked by the storm-wave base, which is about 50 m in dense brines, as proposed by some scholars [47,52,53]. However, the volume within deep water basins is generally huge below the wave base [53], which tends to have large vertical gradients in density in hypersaline settings, resulting in the upper mixed layer and the bottom water being commonly stably stratified [51]. For example, for the deep-water gypsum deposition in the Dead Sea during meromictic periods, the water column remains stably stratified throughout the year.

Although paleo-water depth, as a significant parameter for paleomorphology restoration and tectonic subsidence history analysis in the basin, has always been valued by geologists, its recovery is difficult in international frontier research [54]. However, considering that the geological structure of the Early Jurassic gulf-like sea is similar to that of the present Red Sea [23], both of which are in the stage of intercontinental rifting, the water depth of the former may be in the same range as the latter, which has an average depth of 558 m and a maximum depth of 3039 m. Although such a comparison does not take into account other geological factors, such as sea-level rise and fall, the water depth of the Early Jurassic gulf-shaped sea may have far exceeded the storm-wave base level of the dense brine. Sufficient water depth makes the stratification of brine in the bottom water stable, which reflects that the deep-water genetic model is suitable for explaining the formation mechanism of gypsum rock in the Early Jurassic. It should be pointed out that this interpretation still needs more evidence, such as geochemistry and paleoecology, in the future. In addition, the shallow water genetic model needs the water evaporation to be much larger than the influx, meaning that the water depth must continue to decline, which is inconsistent with the continuous sea level rise from 201 Ma to 183 Ma. Thus, the deep water model for the gypsum within the East African continental margin basins from 201 Ma to 183 Ma could be established. In this model (Figure 11a), with the break-up of the Gondwana continent, the global sea level began to rise. The Paleo-Tethys Ocean first invaded the rifting basin from the northeast to form a gulf-like sea. At this time, the Ruvuma River, the Rufiji River, and the other river systems provided clastic material to the basins, forming a sedimentary system including delta, coastal plain, littoral, and neritic-bathyal environments. As the sea level continued to rise, it exceeded the storm-wave base for dense brines, which tend to have large vertical gradients in density. The bottom water and upper water within the central of the basins, which corresponds to the central of the neritic-bathyal facies, were stably stratified, allowing thin gypsum layers to precipitate. Notably, thin-layered gypsum deposits could be precipitated at the edge of the neritic-bathyal facies due to the suitable depth created by the activities of extensional faults. However, the strong water exchange in the northeastern part impeded stratification, resulting in little precipitation of the gypsum, which is why gypsum deposits are lacking in the Lamu Basin. Vertically, as the sea level continues to rise, the values of TOC and HI increase. The more stable the bottom water layer becomes, the more reducibility becomes stronger.

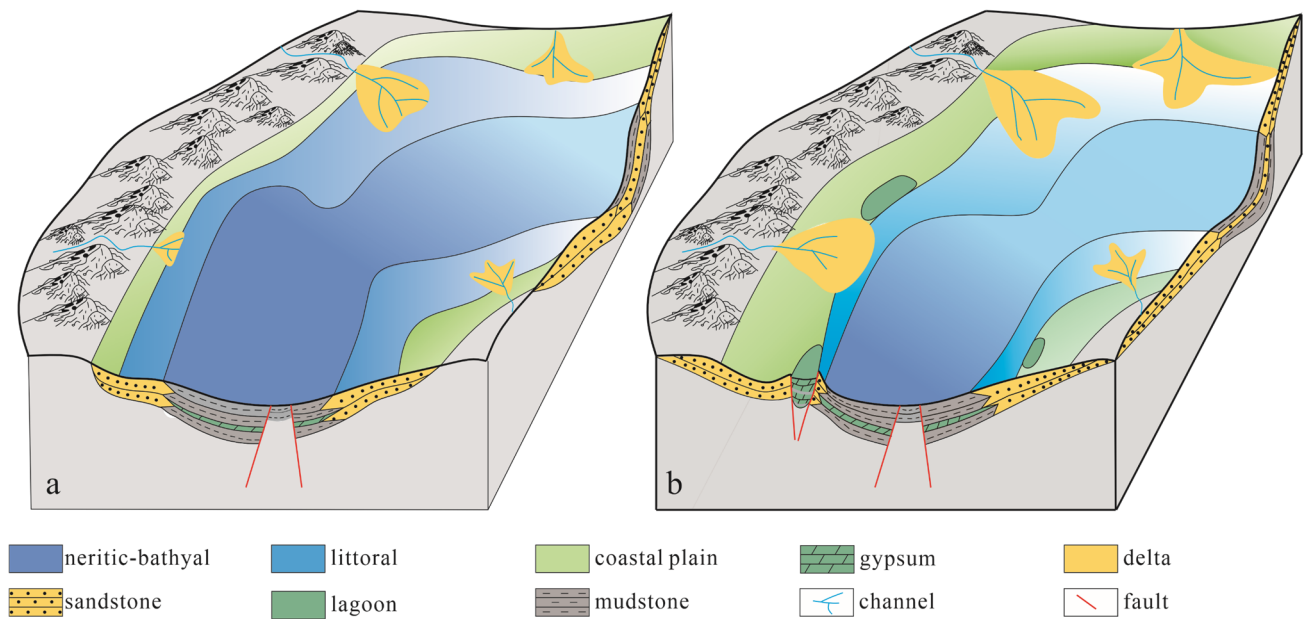


**Figure 11.** (a) A schematic diagram shows the sedimentary model during sea level rise. (b) Schematic diagram showing the sedimentary model during the seal level drawdown.

The sea level within the East Africa continental margin basins began to fall around 183 Ma ago, and the area of the neritic-bathyal environment gradually became smaller. Considering that brine stratification existed in deeper water during this period, the area of gypsum precipitation became limited to the center of the neritic-bathyal environment. However, in terms of the distribution range of a thick suite of gypsum far from the center of the basins, the deep water genetic model is herein difficult to account for its formation. It can be found that the thick gypsum deposits are mainly located in grabens formed by extensional faulting. The grabens provided accommodation space for subsequent thick gypsum deposition, and the rise of the areas adjacent to the grabens limited the influx of seawater, which further resulted in the formation of the lagoons (Figure 11b). As the sea level continued to decline, the brine within lagoons became more concentrated, and then the thick gypsum deposits precipitated.

Although gypsum-bearing basins are widely developed in the world, the model of the Early Jurassic gypsum within the East African continental marginal basins cannot be mechanically applied to other basins. It is necessary to comprehensively consider whether the target basin has a similar tectonic and sedimentary background as the Early Jurassic East African continental marginal basins. For example, whether the gypsum deposits are mainly formed in the intercontinental rift period or whether the gypsum deposit formation period has similar sea level changes. Only by meeting these characteristics can we consider learning from the depositional model of the Early Jurassic gypsum deposits within the East African continental marginal basins.

#### 5.4. Geological Significance for Gas Play

##### 5.4.1. Expanding the Scope of the Hydrocarbon Generation Window

Since the discovery of the first large gas field in the deep-water area of East Africa in 2010, the deep-water areas of Tanzania and Rovuma basins have become one of the hot spots for global deep-water oil and gas exploration due to their huge proven gas reservoir reserves [21]. Geochemical evidence suggests that the Lower Jurassic mudstone is the main source rock for gas reservoirs in the Rovuma and Tanzania Basins [19]. It should be pointed out that conventional thermal history simulations of source rocks reached a peak of gas generation during the Paleocene, followed by a gradual decline in gas production [21],

which makes it difficult to explain the ongoing filling of East African natural gas reservoirs and the formation of giant reserves.

Considering that the gypsum deposits have high thermal conductivity and a low heat generation rate [55], they can transmit ground temperature easily from the deep stratum to the shallow stratum. This may lead to a lower temperature gradient and an abnormally low temperature of the source rock in the lower part of the gypsum stratum than in the non-gypsum stratum. The abnormal temperatures in the lower part of the gypsum stratum result in an increase in the maturity threshold depth of the source rocks and delay the peak time of gas generation. This can effectively expand the scope of the hydrocarbon generation window and may be the reason why giant amounts of natural gas are still continuously accumulating.

#### 5.4.2. Sealing Property and Potential Hydrocarbon Traps

Irrespective of their thickness and geodynamic setting, the gypsum deposits acted as an effective sealing unit [56]. The widely distributed gypsum deposits hinder the upward dissipation of natural gas. Although the main targets for deep-water gas exploration currently in the Rovuma and Tanzania Basins are the Late Cretaceous and Paleogene turbidite sandstones, most of the gas fields are located near the large-scale fault zones connecting the source and the reservoirs, indicating that gas generated from Lower Jurassic source rocks vertically migrated along the large-scale fault zones and accumulated in the turbidite sandstones (Figure 12). Considering that both the Rovuma and Tanzania Basins were dominated by thermal subsidence during the Early Jurassic period, a small number of preexisting faults have been reactivated under the regional extensional stress field, resulting in the formation of some horst-graben structures. The Triassic fluvial and lacustrine sandstones [21] in the horst structures can be used as the pointing area for the near-source dominant migration of natural gas, forming “new source, old reservoir” type buried hills, which should be given more attention in further gas exploration (Figure 12).

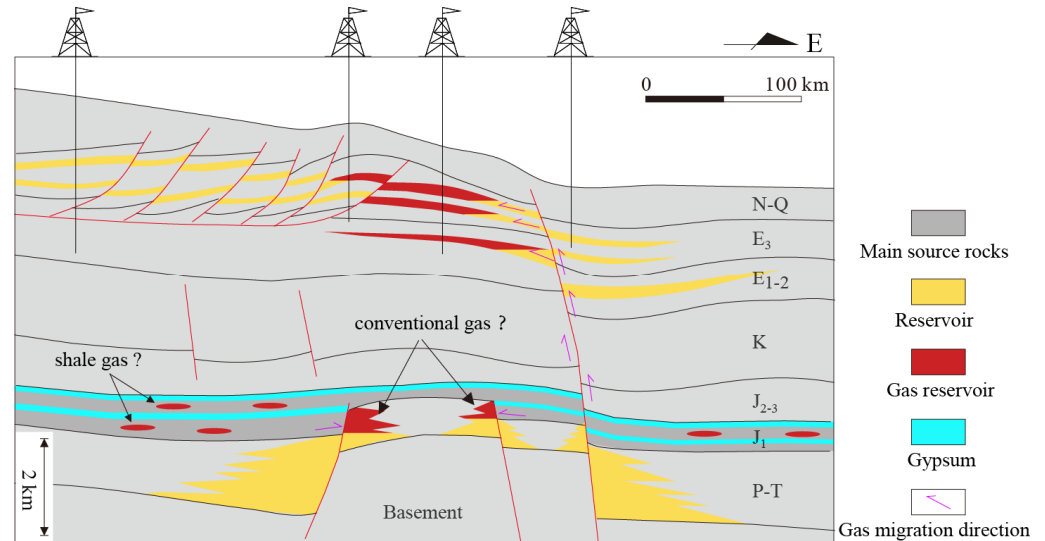


**Figure 12.** The model shows gas migration and accumulation within the Eastern African continental marginal basins.

Because of the good sealing properties of gypsum deposits, most of the discovered gas fields are located near the large-scale fault zones connecting the source and the reservoirs. In addition, the Lower Jurassic shale where the faults are not developed may be rich in a large amount of undischarged shale gas, and the place with a high brittle mineral content will be an important place for shale gas exploration in the future.

## 6. Conclusions

- (1) The thick suite of mudstone with thin-layered gypsum deposits is widely distributed in the Lower Jurassic within the Rovuma and southern Tanzania Basins. The thick suite of gypsum deposits with thin layers of mudstone is mainly distributed in the upper part of the Lower Jurassic, located in grabens formed by extensional faulting.
- (2) With the break-up of the Gondwana continent, the eastern African continental margin basins experienced a sea level rise from 201 Ma to 183 Ma, with a gradual increasing reducibility from northeast of the gulf-like sea to southwest, and then began to fall until the end of the Early Jurassic with a gradual decreasing reducibility.
- (3) The deep-water gypsum genetic model could account for the distribution of the thick suite of mudstone with the thin layers of gypsum deposited during the entire Early Jurassic. The model of the lagoon could account for the limited distribution of the thick suite of gypsum deposits with thin layers of mudstone deposited during the late stage of the Early Jurassic.
- (4) The high thermal conductivity and low heat generation rate of gypsum deposits result in increasing the maturity threshold depth of Lower Jurassic source rocks and delaying the peak time of gas generation. The good sealing of gypsum makes the discovered Late Cretaceous and Paleocene gas fields mainly located near the large-scale fault zones connecting the source and the reservoirs, and the traps of Triassic fluvial and lacustrine sandstones in the horst structures could be potential conventional gas exploration targets, while the Lower Jurassic shale where the faults are not developed may be an important place for shale gas exploration in the future.

**Author Contributions:** J.C.: Conceptualization, methodology, writing, and funding acquisition. R.G.: data curation and formal analysis. All authors have read and agreed to the published version of the manuscript.

**Funding:** This research was financially supported by the National Natural Science Foundation of China (No. 42002150), the Open Foundation of Cooperative Innovation Center of Unconventional Oil and Gas, Yangtze University (Ministry of Education & Hubei Province) (No. UOG2024-12), the Open Foundation Project of the Key Laboratory of Polar Geology and Marine Mineral Resources (China University of Geosciences, Beijing, China), Ministry of Education (No. PGMR-2023-201), and the National Key Research Program of China (No. 2017ZX05032-002).

**Data Availability Statement:** Data is contained within the article.

**Acknowledgments:** We sincerely thank three anonymous reviewers for their critical comments and constructive suggestions, which have greatly improved the quality of this paper.

**Conflicts of Interest:** The authors declare no conflict of interest.

## References

1. Warren, J.K. Evaporites through time: Tectonic, climatic and eustatic controls in marine and nonmarine deposits. *Earth-Sci. Rev.* **2010**, *98*, 217–268. [[CrossRef](#)]
2. Yu, Y.; Tang, L.; Yang, W.; Qiu, N.; Li, W. Salt structures and hydrocarbon accumulations in the Tarim Basin, northwest China. *AAPG Bull.* **2014**, *98*, 135–159. [[CrossRef](#)]
3. Wang, X.; Fei, Q.; Zhang, J. Cenozoic Diapiric Traps in Eastern China. *AAPG Bull.* **1985**, *69*, 2098–2109. [[CrossRef](#)]
4. Zhu, C.; Jiang, F.; Zhang, P.; Zhao, Z.; Chen, X.; Wu, Y.; Chen, Y.; Wang, W.; Song, Z.; Hu, T.; et al. Effect of petroleum chemical fraction and residual oil content in saline lacustrine organic-rich shale: A case study from the Paleogene Dongpu Depression of North China. *Petrol. Sci.* **2023**, *20*, 649–669. [[CrossRef](#)]
5. Fu, L.; Li, J.; Xu, W.; Guo, W.; Li, N.; Zhang, Y.; Song, W.; Sun, Y. Characteristics and main controlling factors of Ordovician deep subsalt reservoir in central and eastern Ordos Basin, China. *J. Nat. Gas Geosci.* **2021**, *6*, 13–25. [[CrossRef](#)]
6. Meng, M.; Ge, H.; Shen, Y.; Ji, W.; Wang, Q. Rock fabric of tight sandstone and its influence on irreducible water saturation in Eastern Ordos Basin. *Energy Fuel* **2023**, *37*, 3685–3696. [[CrossRef](#)]
7. Zhou, J.; Wu, G.; Geng, Y.; Guo, Y.; Chang, X.; Peng, C.; Ai, C. Laboratory study of the factors affecting hydraulic fracturing effect for inter-salt oil shale layers, Qianjiang Depression, China. *Petrol. Sci.* **2023**, *20*, 1690–1706. [[CrossRef](#)]
8. Meng, M.; Ge, H.; Shen, Y.; Wang, L. Influence of rock fabric on salt ion diffusion behavior in upper cretaceous lacustrine shale from Songliao Basin. *J. Petrol. Sci. Eng.* **2022**, *208*, 109355. [[CrossRef](#)]

9. Meng, M.; Peng, J.; Ge, H.; Ji, W.; Li, X.; Wang, Q. Rock Fabric of Lacustrine Shale and Its Influence on Residual Oil Distribution in the Upper Cretaceous Qingshankou Formation, Songliao Basin. *Energy Fuel* **2023**, *37*, 7151–7160. [[CrossRef](#)]
10. Liang, C.; Ding, W.; Liu, Y.; Li, M. The Late Cretaceous—Miocene supra-salt structures in Block M, Lower Congo Basin (Congo, West Africa) and the controls on channel development. *Geol. J.* **2022**, *57*, 4167–4182. [[CrossRef](#)]
11. Edgell, H.S. Salt tectonism in the Persian Gulf basin. *Geol. Soc. Lond. Spec. Publ.* **1996**, *100*, 129–151. [[CrossRef](#)]
12. Hassanpour, J.; Yassaghi, A.; Muñoz, J.A.; Jahani, S. Salt tectonics in a double salt-source layer setting (Eastern Persian Gulf, Iran): Insights from interpretation of seismic profiles and sequential cross-section restoration. *Basin Res.* **2021**, *33*, 159–185. [[CrossRef](#)]
13. Volozh, Y.; Talbot, C.; Ismail-Zadeh, A. Salt structures and hydrocarbons in the Pricaspian basin. *AAPG Bull.* **2003**, *87*, 313–334. [[CrossRef](#)]
14. Jackson, M.P.; Hudec, M.R.; Jennette, D.C.; Kilby, R.E. Evolution of the Cretaceous Astrid thrust belt in the ultradeep-water Lower Congo Basin, Gabon. *AAPG Bull.* **2008**, *92*, 487–511. [[CrossRef](#)]
15. Quirk, D.G.; Schødt, N.; Lassen, B.; Ings, S.J.; Hsu, D.; Hirsch, K.K.; Von Nicolai, C. Salt tectonics on passive margins: Examples from Santos, Campos and Kwanza basins. *Geol. Soc. Lond. Spec. Publ.* **2012**, *363*, 207–244. [[CrossRef](#)]
16. Adam, J.; Ge, Z.; Sanchez, M. Salt-structural styles and kinematic evolution of the Jequitinhonha deepwater fold belt, central Brazil passive margin. *Mar. Petrol. Geol.* **2012**, *37*, 101–120. [[CrossRef](#)]
17. Alves, T.M.; Fetter, M.; Lima, C.; Cartwright, J.A.; Cosgrove, J.; Gangá, A.; Queiroz, C.L.; Strugale, M. An incomplete correlation between pre-salt topography, top reservoir erosion, and salt deformation in deep-water Santos Basin (SE Brazil). *Mar. Petrol. Geol.* **2017**, *79*, 300–320. [[CrossRef](#)]
18. Qin, P.; Zhong, D.; Su, C.; Mo, T.; Tang, Y. Effect of the internal plastic deformation of salt structures on the lithologic succession of evaporites: A case study on the Palaeogene Kumugeliemuqun formation, Kelasu Thrust Belt, Kuqa depression, Tarim Basin. *J. Petrol. Sci. Eng.* **2022**, *208*, 109559. [[CrossRef](#)]
19. Sun, Y.; Sun, T.; Xu, Z. Source rock characteristics and oil-gas origins in Tanzania basin, East Africa coast. *China Offshore Oil Gas* **2016**, *28*, 13–19. [[CrossRef](#)]
20. Liang, J.; Kong, L.; Qiu, C.; Li, H.; Jia, S.; Long, X. Gas accumulation mechanism in East Africa coastal key basins. *Earth Sci.* **2021**, *46*, 2919–2933. [[CrossRef](#)]
21. Bird, D.E.; Burke, K.; Hall, S.A.; Casey, J.F. Gulf of Mexico tectonic history: Hotspot tracks, crustal boundaries, and early salt distribution. *AAPG Bull.* **2005**, *89*, 311–328. [[CrossRef](#)]
22. Catuneanu, O.; Wopfner, H.; Eriksson, P.G.; Cairncross, B.; Rubidge, B.S.; Smith RM, H.; Hancox, P.J. The Karoo basins of south-central Africa. *J. Afr. Earth Sci.* **2005**, *43*, 211–253. [[CrossRef](#)]
23. Deng, Y. Discussion on the control effect of gulf on marine petroleum. *Acta Pet. Sin.* **2018**, *39*, 1–11. [[CrossRef](#)]
24. Reeves, C. Re-examining the evidence from plate-tectonics for the initiation of Africa’s passive margins. In Proceedings of the Geological Society of Houston/Petroleum Exploration Society of Great Britain, London, UK, 9–10 September 2009.
25. Geiger, M.; Clark, D.N.; Mette, W. Reappraisal of the timing of the breakup of Gondwana based on sedimentological and seismic evidence from the Morondava Basin, Madagascar. *J. Afr. Earth Sci.* **2004**, *38*, 363–381. [[CrossRef](#)]
26. Key, R.M.; Smith, R.A.; Smelror, M.; Sæther, O.M.; Thorsnes, T.; Powell, J.H.; Njange, F.; Zandamela, E.B. Revised lithostratigraphy of the Mesozoic-Cenozoic succession of the onshore Rovuma Basin, northern coastal Mozambique. *S. Afr. J. Geol.* **2008**, *111*, 89–108. [[CrossRef](#)]
27. Mougénot, D.; Recq, M.; Virlogeux, P.; Lepvrier, C. Seaward extension of the East African Rift. *Nature* **1986**, *321*, 599–603. [[CrossRef](#)]
28. Cai, J.; Luo, S.; Guan, Y.; Dong, P. Main controlling factors of organic matter enrichment of the Mesoproterozoic source rocks from the North China Craton. *Geol. J.* **2021**, *56*, 422–433. [[CrossRef](#)]
29. Neal, J.; Abreu, V. Sequence stratigraphy hierarchy and the accommodation succession method. *Geology* **2009**, *37*, 779–782. [[CrossRef](#)]
30. Zhang, M.; Zhang, J.; Xu, F.; Li, J.; Liu, J.; Hou, G.; Zhang, P. Paleocene sequence stratigraphy and depositional systems in the Lishui Sag, East China Sea Shelf Basin. *Mar. Petrol. Geol.* **2015**, *59*, 390–405. [[CrossRef](#)]
31. Haq, B.U.; Hardenbol, J.; Vail, P.R. Chronology of fluctuating sea levels since the Triassic. *Science* **1987**, *235*, 1156–1167. [[CrossRef](#)]
32. Phethean, J.J.; Kalnins, L.M.; van Hunen, J.; Biffi, P.G.; Davies, R.J.; Mccaffrey, K.J. Madagascar’s escape from Africa: A high-resolution plate reconstruction for the Western Somali Basin and implications for supercontinent dispersal. *Geochem. Geophys. Geosyst.* **2016**, *17*, 5036–5055. [[CrossRef](#)]
33. Scotese, C.R. Jurassic and Cretaceous plate tectonic reconstructions. *Palaeogeogr. Palaeoclimatol. Palaeoecol.* **1991**, *87*, 493–501. [[CrossRef](#)]
34. Schoepfer, S.D.; Shen, J.; Wei, H.; Tyson, R.V.; Ingall, E.; Algeo, T.J. Total organic carbon, organic phosphorus, and biogenic barium fluxes as proxies for paleomarine productivity. *Earth-Sci. Rev.* **2015**, *149*, 23–52. [[CrossRef](#)]
35. Arthur, M.A.; Dean, W.E.; Pratt, L.M. Geochemical and climatic effects of increased marine organic carbon burial at the Cenomanian/Turonian boundary. *Nature* **1988**, *335*, 714–717. [[CrossRef](#)]
36. Hedges, J.I.; Keil, R.G. Sedimentary organic matter preservation: An assessment and speculative synthesis. *Mar. Chem.* **1995**, *49*, 81–115. [[CrossRef](#)]
37. Demaison, G.J.; Moore, G.T. Anoxic environments and oil source bed genesis. *Org. Geochem.* **1980**, *2*, 9–31. [[CrossRef](#)]

38. Degens, E.T.; von Herzen, R.P.; Wong, H.; Deuser, W.G.; Jannasch, H.W. Lake Kivu: Structure, chemistry and biology of an East African rift lake. *Geol. Rundsch.* **1973**, *62*, 245–277. [[CrossRef](#)]
39. Mazzini, A.; Ivanov, M.K.; Nermoen, A.; Bahr, A.; Bohrmann, G.; Svensen, H.; Planke, S. Complex plumbing systems in the near subsurface: Geometries of authigenic carbonates from Dolgovskoy Mound (Black Sea) constrained by analogue experiments. *Mar. Petrol. Geol.* **2008**, *25*, 457–472. [[CrossRef](#)]
40. Jin, Q.; Zhu, G.; Wang, J. Deposition and distribution of high-potential source rocks in saline lacustrine environments. *J. China Univ. Pet.* **2008**, *32*, 19–23. [[CrossRef](#)]
41. Wei, H.; Jiang, X. Early Cretaceous ferruginous and its control on the lacustrine organic matter accumulation: Constrained by multiple proxies from the Bayingebi Formation in the Bayingebi Basin, inner Mongolia, NW China. *J. Petrol. Sci. Eng.* **2019**, *178*, 162–179. [[CrossRef](#)]
42. Katz, B.J. Controls on distribution of lacustrine source rocks through time. *AAPG Mem.* **1990**, *50*, 132–139.
43. Talbot, M.R.; Livingstone, D.A. Hydrogen index and carbon isotopes of lacustrine organic matter as lake level indicators. *Palaeogeogr. Palaeoclimatol. Palaeoecol.* **1989**, *70*, 121–137. [[CrossRef](#)]
44. Hsü, K.J. Origin of saline giants: A critical review after the discovery of the Mediterranean evaporite. *Earth-Sci. Rev.* **1972**, *8*, 371–396. [[CrossRef](#)]
45. Hsü, K.J.; Ryan, W.B.; Cita, M.B. Late Miocene desiccation of the Mediterranean. *Nature* **1973**, *242*, 240–244. [[CrossRef](#)]
46. Brongersma-Sanders, M. Origin of major cyclicity of evaporites and bituminous rocks: An actualistic model. *Mar. Geol.* **1971**, *11*, 123–144. [[CrossRef](#)]
47. Christeleit, E.C.; Brandon, M.T.; Zhuang, G. Evidence for deep-water deposition of abyssal Mediterranean evaporites during the Messinian salinity crisis. *Earth Planet. Sci. Lett.* **2015**, *427*, 226–235. [[CrossRef](#)]
48. Debenedetti, A. The problem of the origin of the salt deposits in the Mediterranean and of their relations to the other salt occurrences in the Neogene formations of the contiguous regions. *Mar. Geol.* **1982**, *49*, 91–114. [[CrossRef](#)]
49. Schmalz, R.F. Deep-water evaporite deposition: A genetic model. *AAPG Bull.* **1969**, *53*, 798–823. [[CrossRef](#)]
50. Schmalz, R.F. The Mediterranean salinity crisis: Alternative hypotheses. *Carbonate Evaporite* **1991**, *6*, 121–126. [[CrossRef](#)]
51. Brainerd, K.E.; Gregg, M.C. Surface mixed and mixing layer depths. *Deep Sea Res. Part I Oceanogr. Res. Pap.* **1995**, *42*, 1521–1543. [[CrossRef](#)]
52. Dietz, R.S. Wave-base, marine profile of equilibrium, and wave-built terraces: A critical appraisal. *Geol. Soc. Am. Bull.* **1963**, *74*, 971–990. [[CrossRef](#)]
53. Sonnenfeld, P. *Models of Upper Miocene Evaporite Genesis in the Mediterranean Region*; Springer: New York, NY, USA, 1985; pp. 323–346.
54. Plint, A.G.; Tyagi, A.; Hay, M.J.; Varban, B.L.; Zhang, H.; Roca, X. Clinoforms, paleobathymetry, and mud dispersal across the Western Canada Cretaceous foreland basin: Evidence from the Cenomanian Dunvegan Formation and contiguous strata. *J. Sediment. Res.* **2009**, *79*, 144–161. [[CrossRef](#)]
55. O'Brien, J.J.; Lerche, I. The influence of salt domes on paleotemperature distributions. *Geophysics* **1984**, *49*, 2032–2043. [[CrossRef](#)]
56. Liu, W.; Zhao, H.; Liu, Q.; Zhou, B.; Zhang, D.; Wang, J.; Lu, L.; Luo, H.; Meng, Q.; Wu, X. Significance of gypsum-salt rock series for marine hydrocarbon accumulation. *Pet. Res.* **2016**, *37*, 1451–1462. [[CrossRef](#)]

**Disclaimer/Publisher's Note:** The statements, opinions and data contained in all publications are solely those of the individual author(s) and contributor(s) and not of MDPI and/or the editor(s). MDPI and/or the editor(s) disclaim responsibility for any injury to people or property resulting from any ideas, methods, instructions or products referred to in the content.